Histol Histopathol (2021) 36: 577-586

http://www.hh.um.es

Histology and Histopathology
From Cell Biology to Tissue Engineering

ORIGINAL ARTICLE **Open Access**

High-resolution three-dimensional visualization of hepatic sinusoids in cirrhotic rats via serial histological sections

Jing-Yi Liu[1], Wen-Juan Lv[1], Jian-Bo Jian[2], Xiao-Hong Xin[1], Xin-Yan Zhao[3,4] and Chun-Hong Hu[1]

[1]School of Biomedical Engineering and Technology, Tianjin Medical University, [2]Department of Radiation Oncology, Tianjin Medical University General Hospital, Tianjin, [3]Liver Research Center, Beijing Friendship Hospital, Capital Medical University and [4]Beijing Key Laboratory of Translational Medicine in Liver Cirrhosis and National Clinical Research Center of Digestive Disease, Beijing, China

Summary. Aim. As a specialized intraparenchymal vascular conduit, hepatic sinusoids play a key role in liver microcirculation. This study aimed to explore the three-dimensional (3D) morphological changes of cirrhotic sinusoids by serial histological sections.

Methods. Cirrhosis was induced by tail vein injection of albumin in Wistar rats with a positive antibody. A total of 356 serial histological sections were prepared from liver tissue blocks of normal and cirrhotic rats. The optical microscope images were registered and reconstructed, and 3D reconstructions of the fine structures of fibrous tissues and sinusoids were subsequently visualized.

Results. The fibrosis area of the cirrhotic sample was 6-16 times that of the normal sample ($P<0.001$). Cirrhosis led to obvious changes in the distribution and morphology of sinusoids, which were mainly manifested as dilation, increased quantity and disordered distribution. Compared with normal liver, cirrhotic liver has a significantly increased volume ratio, number and volume of sinusoids (1.63-, 0.53-, and 1.75-fold, respectively, $P<0.001$). Furthermore, the samples were further divided into three zones according to the oxygen supply, and there were significant differences in the morphology of the sinusoids in the normal and cirrhotic samples ($P<0.05$). In particular, morphological parameters of the cirrhotic sinusoids near the portal area were obviously greater than those in the normal liver ($P<0.05$).

Conclusion. 3D morphological structures of hepatic sinusoids were reconstructed, and the adaptive microstructure changes of cirrhotic sinusoids were accurately measured, which has an important implications for the study of hepatic microcirculation and pathological changes of cirrhosis.

Key words: 3D reconstruction, Cirrhosis, Hepatic sinusoids, Pathology

Corresponding Author: Chun-Hong Hu PhD., School of Biomedical Engineering and Technology, Tianjin Medical University, Tianjin 300070, China. e-mail: chunhong_hu@hotmail.com or Xin-Yan Zhao PhD., Liver Research Center, Beijing Friendship Hospital, Capital Medical University, Beijing100050, China. e-mail: zhao_xinyan@ccmu.edu.cn

DOI: 10.14670/HH-18-339

Introduction

Liver disease is a major cause of illness and death worldwide. In China, different types of liver diseases affect approximately 300 million people (Wang et al., 2014). The liver possesses an extraordinary ability to regenerate after injury. The regulatory mechanism of blood vessel and cell regeneration in the liver has always been a research topic, and it has attracted much attention. However, as specialized intraparenchymal vascular conduits (Brunt et al., 2014), the function of hepatic sinusoids is still largely unknown. Hepatic sinusoids play important roles in hepatic microcirculation. Under normal physiological conditions, nutrient-rich venous blood and oxygen-rich arterial blood combine and flow through the sinusoids (Rappaport et al., 1966). Under pathological conditions, different diseases may result in physically altered, usually enlarged, sinusoids (Brunt et al., 2014). Morphological changes such as sinusoidal dilation correlate with microcirculation in the liver. Hepatic sinusoids are strongly related to the pathogenesis of liver cirrhosis (Zhang et al., 2020), and cirrhosis causes morphological and pathological changes in sinusoids.

At present, researchers have used confocal laser scanning microscopy (CLSM) with submicron spatial resolution to assess hepatic sinusoids, but liver tissue slices are limited to being approximately 150-μm thick due to technical limitations (Hoehme et al., 2010).

Recently, structural alterations of sinusoids, such as those to the diameter, perimeter and sinusoidal endothelial cell structure, have been reported by different microscopy techniques (Onori et al., 2000; Vollmar and Menger, 2009; Duan et al., 2013a,b; Yoon et al., 2013), such as high-resolution light microscopy (LM), transmission electron microscopy (TEM), and scanning electron microscopy (SEM). In practice, these imaging methods can provide extraordinary spatial resolution on micron and nanometre scales, but these traditional microscopes provide information about the surface or to very shallow depths. By more contemporary electron modalities, scholars have used serial block-face scanning electron microscopy (SBF-SEM) to quantify geometric bile canaliculi properties from three dimensional (3D) models of the single bile canaliculus (Meyer et al., 2017). Also, array tomography has been used to generate cross-sections of murine infrarenal aorta (Saatchi et al., 2011) and zebrafish's entire liver (Cheng et al., 2019) and so on, which disclose large-volume structural information at the nanometre resolution. But a major challenge of SBF-SEM is electron charging, which results in a range of undesirable artifacts (Titze and Genoud, 2016), and array tomography procedures are relatively complex and demanding (Micheva et al., 2010). High-resolution microcomputed tomography (Micro-CT) can realize the imaging of new capillaries and sinusoids in mice with the help of angiography (Cheng et al., 2017). Combining the complementarity of both vascular corrosion casting (VCC) (with Micro-CT scanning and contrast agent) and immunohistochemistry (IHC) (with confocal imaging) enables the setup of multilevel models of the microvasculature of the rat liver (Peeters et al., 2017). Previous studies have used synchrotron radiation technology to perform 3D imaging of human hepatic sinusoids; however, the microstructure of normal hepatic sinusoids is invisible under an imaging resolution of 9 μm without using contrast agents (Duan et al., 2013a,b). Similarly, 3D images of hepatic sinusoids and their alterations associated with acute liver injury with X-ray contrast agent at 1-μm resolution have been visualized using synchrotron radiation micro-computed tomography, but the horizontal field of view is limited to 580 μm (Yoon et al., 2013). Although magnetic resonance imaging (MRI) and computed tomography (CT) have been significantly improved, they do not yield satisfactory resolution for life science research. As the diagnostic gold standard, histopathology has excellent resolution and always plays an important role in clinical diagnosis, but it cannot obtain 3D information. Combining 3D visualization techniques with serial histological sections, the 3D morphology of the inner microstructure of a large liver sample can be presented with submicron resolution. In recent decades, biliary tree, hepatic artery branches, lymphatic vessels, portal tract and the individual parenchymal units have been visualized in 3D by serial histological sections (Adams et al., 1974; Nonomura et al., 1978; Teutsch et al., 1999). The 3D structure of the liver sinusoids in cirrhotic samples was reconstructed using only 20 serial sections (Shimizu et al., 1996). With the further development of technology, this technique has been widely utilized to obtain high-resolution 3D structures of samples of breast cancer, prostate cancer, bladder tumors, oral tongue squamous cell carcinoma, and jaw fibrous bone lesions (Araki et al., 2010; Booth et al., 2015; Tolkach et al., 2018; Wang et al., 2018; Jansen et al., 2019).

In this study, a 3D reconstruction technique using serial histological sections was used to visualize the hepatic sinusoids of normal and cirrhotic rats. The morphological structures of sinusoids were presented, such as dilation, elongation and deformation of hepatic sinusoids in cirrhotic rat, and the related anatomical characteristics of sinusoids, including volume, quantity and volume ratio, were investigated. The aim was to explore 3D morphological changes in hepatic sinusoids caused by cirrhosis through serial histological sections.

Materials and methods

Sample preparation

The animal experiments were performed in accordance with the guiding principles for the care and use of laboratory animals approved by the Research Ethics Committee of the Beijing Friendship Hospital, Capital Medical University, China. Male Wistar rats weighing 120-150g were maintained in an environmentally controlled room (23±2°C, 55±10% humidity) with a 12 hour light/dark cycle and free access to food and water. Rats were sensitized by subcutaneous injection of Freund's adjuvant and albumin, followed by human serum albumin attacking via tail vein injection (Wang, 1989; Zhao et al., 2008; Nie et al., 2010). Normal group was injected with normal saline as control. Normal and cirrhotic rats were intraperitoneally anesthetized with 0.6% pentobarbital sodium (PBS). Liver tissues were perfused by PBS and the left lobe was taken out and fixed with 10% neutral formalin (immersion). A histological standard published previously was utilized for semi quantification of experimental liver fibrosis and classified the degree of fibrosis into 7 stages (0-6) (Zhao et al., 2008). According to this standard, cirrhotic samples defined as broad fibrosis bands and multiple complete nodules (Stage 5 or 6) were used for subsequent experiments in this study. Normal and cirrhotic livers were used to prepare serial sections and for follow-up studies.

Serial histological section and staining

The serial sections used in this study were carried out with the assistance of the Pathology Department of Beijing China-Japan Friendship Hospital and Japan Medical University. A total of 356 serial histological sections (4 μm thick) were prepared from every tissue block by an experienced pathologist. Sections were

sequentially numbered in order in case of missing tissue and stained by Masson.

Digitisation of the histological slides

All histological sections were digitized with PANNORAMIC Diagnostic Scanner (3DHISTECH Ltd, Budapest, Hungary) with 20×objectives (PLAN-APOCHROMAT 20× N.A.0.8, resolution 0.23 μm/pixel), and all images were saved with a 100% quality factor setting in histoscanner-specific MRXS image format. No image compression was performed during scanning and storage, and 71 GB of data in total was obtained. CaseViewer (3DHISTECH, Budapest, Hungary) software was used for section viewing.

Image pre-processing and registration

The purpose of medical image registration is to match all anatomical points or diagnostically meaningful points of two images. Historically, image registration can be classified as either "rigid" and "non-rigid" (Crum et al., 2004). Rigid registration is not suitable for non-rigid or non-linear objects, and deformation during the preparation of biological soft tissue sections is inevitable. Therefore, non-rigid registration was selected in this study.

Before registration, image pre-processing was used to adjust the greyscale contrast. First, to eliminate the effects of uneven dyeing in histological sections, the collagen tissues stained blue were selected and then replaced with black. Then the "Image-Adjustments-Black&White" function in Adobe Photoshop CS6 (Adobe Systems, San Jose, CA, USA) was used to convert color images to grayscale and the option "Maximum Black" was used to maximize the contrast between the sinusoids and the parenchyma. During this process, all images are uncompressed and saved with a quality factor of 100%.

In this study, an elastic deformation registration method based on the b-spline algorithm (Carazo et al., 2006) was used via ImageJ (Wayne Rasband, National Institutes of Health, USA) (Schneider et al., 2012) software. For N images, the (N/2) th image was selected as the target image to minimize the cumulative error in the registration process. Furthermore, to reduce artificial errors in the process of manual delineation of the region of interest (ROI), the complete sections were registered. For each sample, the 356 sections were divided into two parts: the first 170 sections were used as the test set, and the remaining sections were used as the validation set.

3D reconstruction

The 3D reconstruction, including surface reconstruction and volume reconstruction, was performed using Amira 6.3 (FEI, Thermo Fisher Scientific, Bordeaux, France). The flowchart of 3D reconstruction is shown in Fig. 1. The threshold segmentation and region growth algorithms were used to connect two-dimensional (2D) contours to generate a

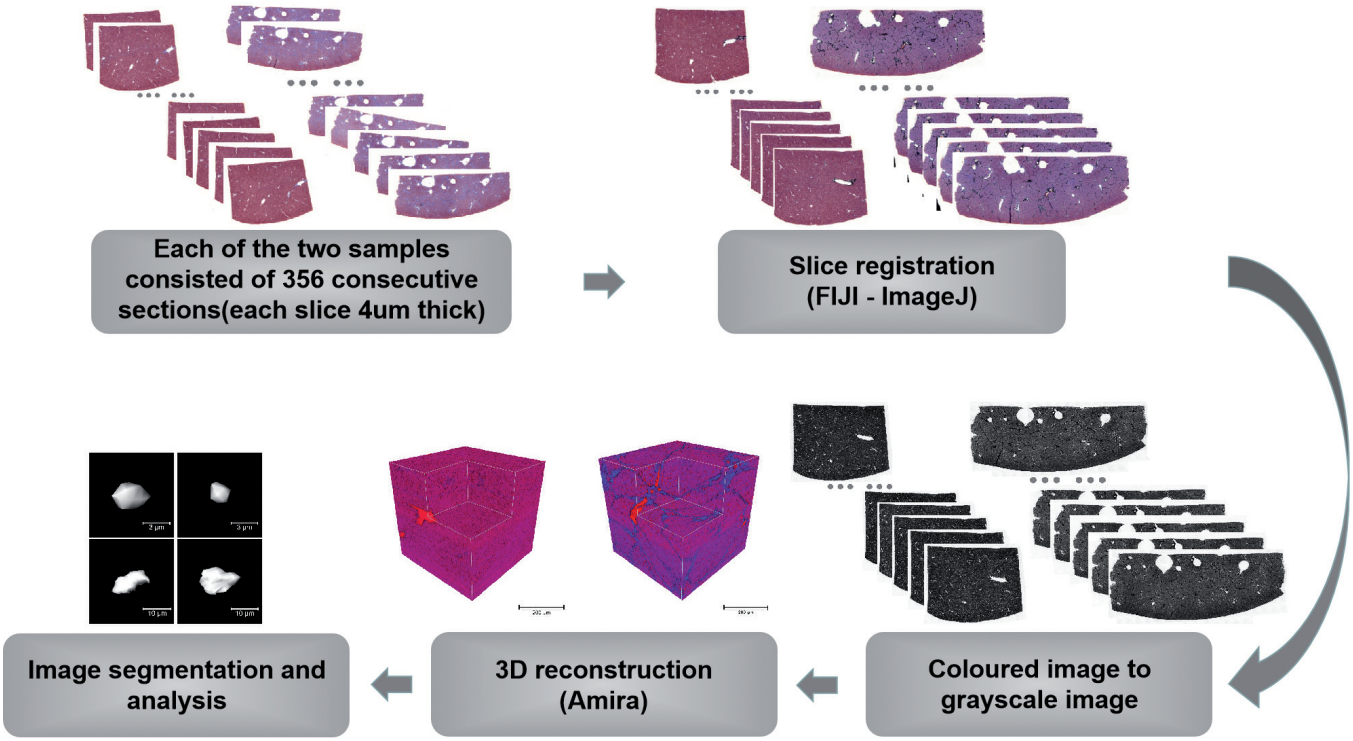

Fig. 1. The flowchart of 3D reconstruction via serial histological sections.

smooth 3D surface. Volume reconstruction technology was used to perform pseudo-color rendering of the structure through different color transfer functions.

Image analysis

Functionally, the liver can be divided into three zones based on oxygen supply. Zone I encircles the portal area where the oxygen-rich blood from hepatic arteries enters, zone III is located around central veins where oxygenation is poor, and zone II is located in between (Kleiner, 2009; Tanaka et al., 2014). In this study, zone I is defined as the surrounding area within 200 μm of the portal area, the adjacent surrounding area up to 400 μm excluding zone I is zone II, and zone III is defined as the region away from the portal area. The sinusoidal volume fraction, number of sinusoids and sinusoid volume in different zones were analysed.

The volume of interest (VOI), with a size of 460*460*460 μm^3, was randomly selected, and the collagen proportinal area from 10 sections of cirrhotic samples was measured. The fibrosis area is given as the proportion of the collagen area of the total area (%). The morphological parameters include sinusoidal volume ratio, number of sinusoids, and single sinusoid volume. Sinusoidal volume ratio refers to the ratio of hepatic sinusoidal volume to total VOI volume. In the morphological analysis of the three zones, ten VOIs with a size of 50*50*50 μm^3 were randomly selected from each zone, and quantitative analysis was performed based on these VOIs.

Statistical analysis

All statistical analyses were performed using the SPSS 25.0 software package (IBM, Chicago, USA). The data conforming to the normal distribution are reported as the means±standard deviation. P values were calculated from Student's t-test. A P value of less than 0.05 was considered to be statistically significant.

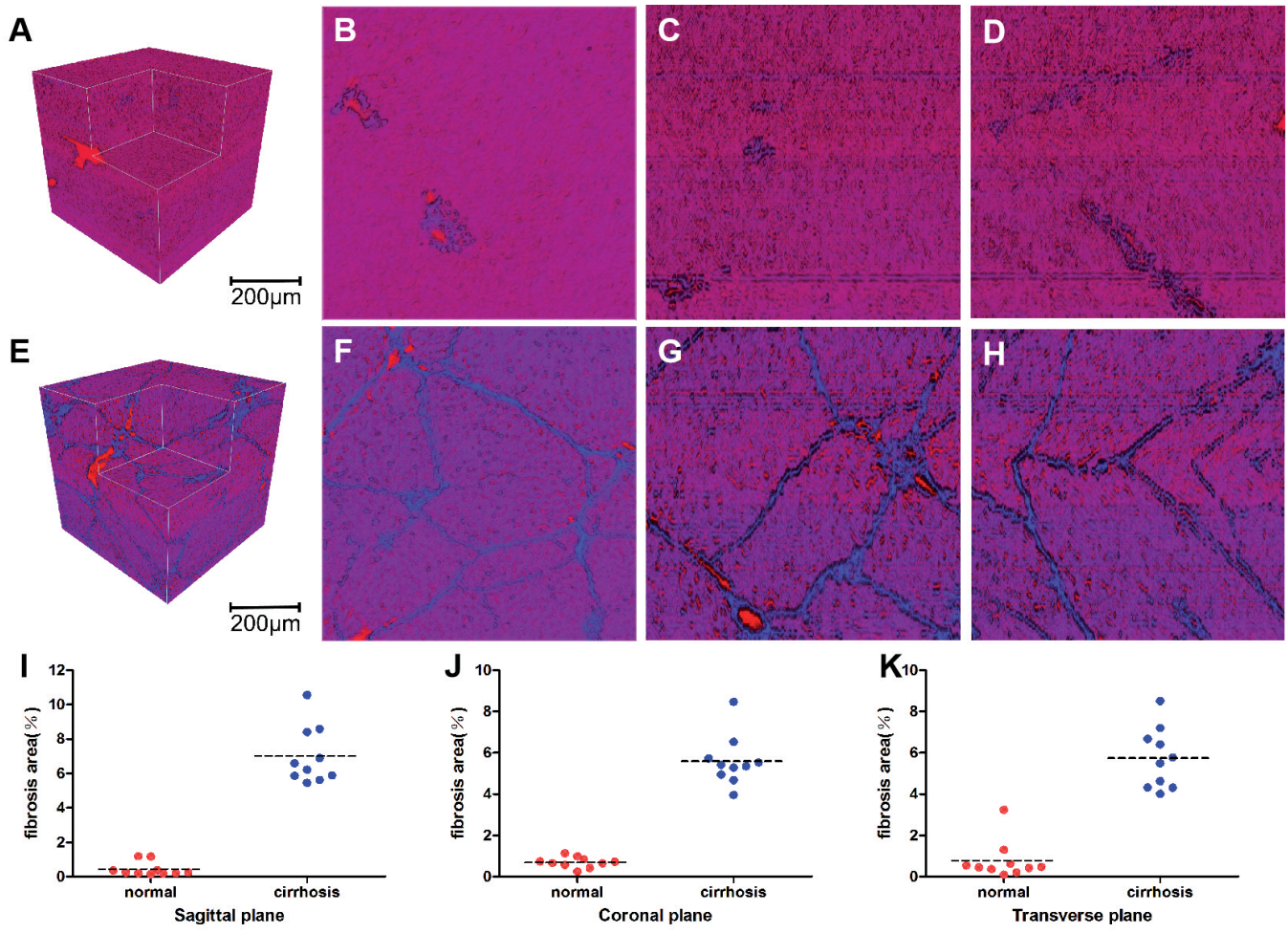

Fig. 2. Illustration and quantification of fibrosis in different directions. 3D reconstruction images of normal and cirrhotic samples are presented in **A** and **E**, and the cross-sections in the sagittal **(B, F)**, coronal **(C, G)**, and transverse **(D, H)** planes are shown. Fibrosis areas were summarized and shown for different samples of sagittal **(I)**, coronal **(J)** and transverse **(K)** planes.

Results

Measurement of fibrosis area in different directions

Figure 2A,E shows local 3D reconstruction of normal and cirrhotic samples, and the sections in the sagittal (Fig. 2B,F), coronal (Fig. 2C,G) and transverse (Fig. 2D,H) planes are presented. In the cirrhotic sample, the fibrosis areas in different directions were 7.01±1.66% (sagittal), 5.58±1.22% (coronal) and 5.74±1.47% (transverse), which significantly increased compared with the normal sample (0.43±0.40% (sagittal), 0.70±0.26% (coronal) and 0.77±0.92% (transverse), respectively, all $P<0.001$), as shown in Fig. 3I-K. Fibrosis areas of cross-sections in different directions were slightly different, and the fibrosis area of the cirrhotic sample was 6-16 times the value of the normal sample.

Distribution of hepatic sinusoids of the periportal and pericentral areas

The sections of normal and cirrhotic samples are shown in Fig. 3A,B. The magnified views of the pericentral and periportal areas in the yellow squares in Fig. 3A,B are shown in Figure 3C-F, and the corresponding 3D volume rendering of the magnified areas are presented in Fig. 3G-J. In the pericentral area, a radial distribution of sinusoids in the normal liver was observed around the central vein (Fig. 3G). In contrast, the sinusoids in cirrhosis presented a uniform distribution with no obvious radial pattern (Fig. 3I). In the periportal area, hepatic sinusoids of normal and cirrhotic livers presented a uniform distribution (Fig. 3H,J).

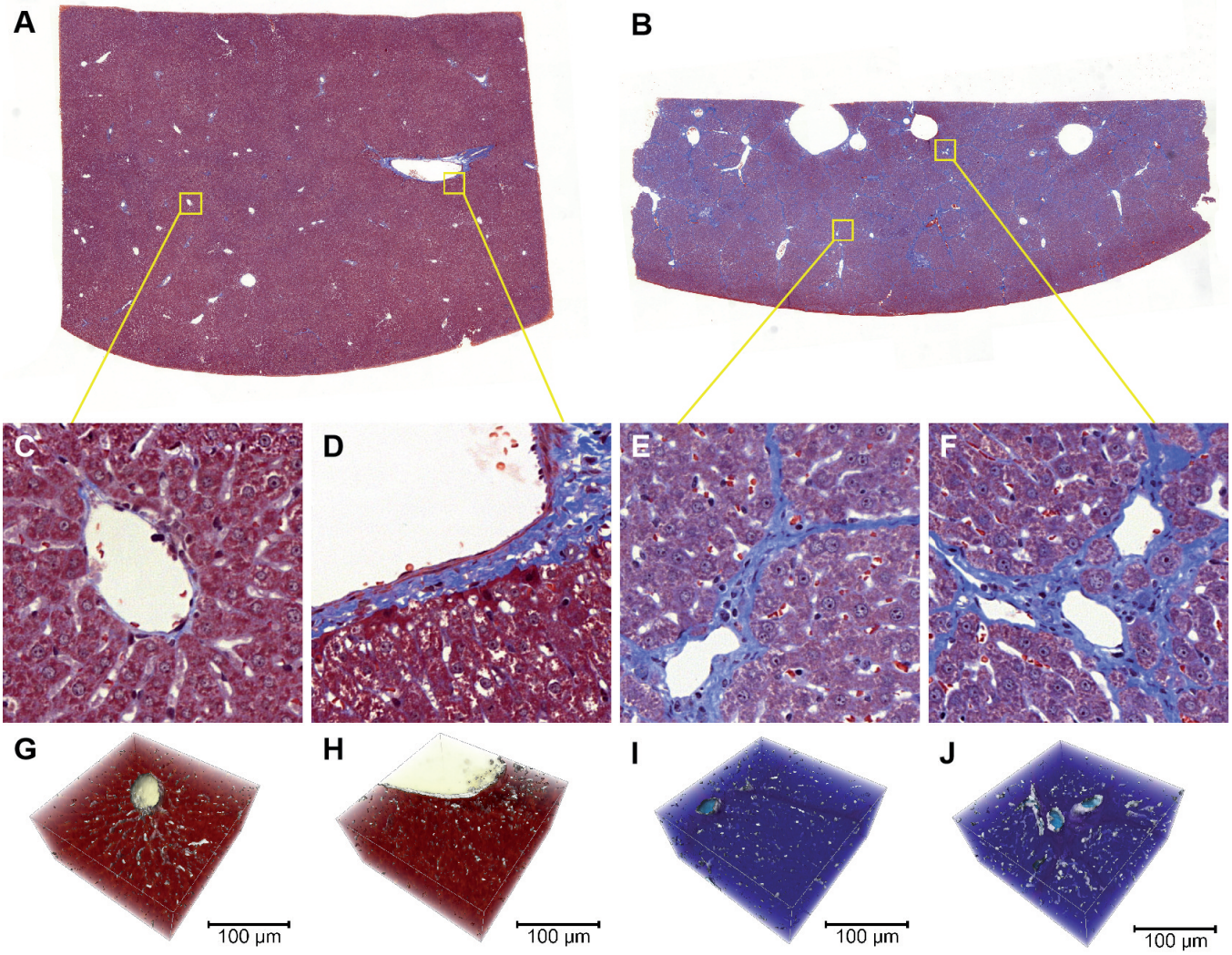

Fig. 3. The hepatic sinusoid distribution in the periportal and pericentral areas. In the section of normal sample **(A)**, the regions near pericentral **(C)** and periportal **(D)**, which are highlighted in the yellow square of Fig. A, were selected for 3D reconstruction **(G, H)**. Similarly, in the sections of the cirrhotic sample (**B**), most of the classic lobular structure was destroyed, and the 3D reconstruction of pericentral **(E)** and periportal **(F)** areas in the yellow squares in Fig. B are presented in **I-J**, respectively.

3D visualization and quantitative measurement of hepatic sinusoids

The 3D distribution of hepatic sinusoids in normal and cirrhotic rats is clearly presented in Fig. 4A,B. Individual sinusoids were chosen randomly and segmented from normal (Fig. 4C) and cirrhotic samples (Fig. 4D). Morphologically, cirrhotic sinusoids are very different from normal sinusoids. Normal sinusoids are smooth, oval and similar in size (Fig. 4c1-c6), while cirrhotic sinusoids are expanded (Fig. 4d1,d2), elongated (Fig. 4d3,d4) and deformed (Fig. 4d5,d6). In addition, the volume, shape, and surface roughness of sinusoids in cirrhosis have also changed. In quantity, there was an obvious increase in cirrhotic sinusoids compared with normal sinusoids (Fig. 4F). Quantitative measurements showed that the volume ratio, number and volume of sinusoids in cirrhotic liver were 2.63- 1.53- and 2.75-fold that of normal liver, respectively (Fig. 4E-G).

Morphological changes of hepatic sinusoids at different zones

Schematic diagrams of zone division in normal and cirrhotic samples are shown in Fig. 5A,B, and representative 3D reconstructions of the three zones are

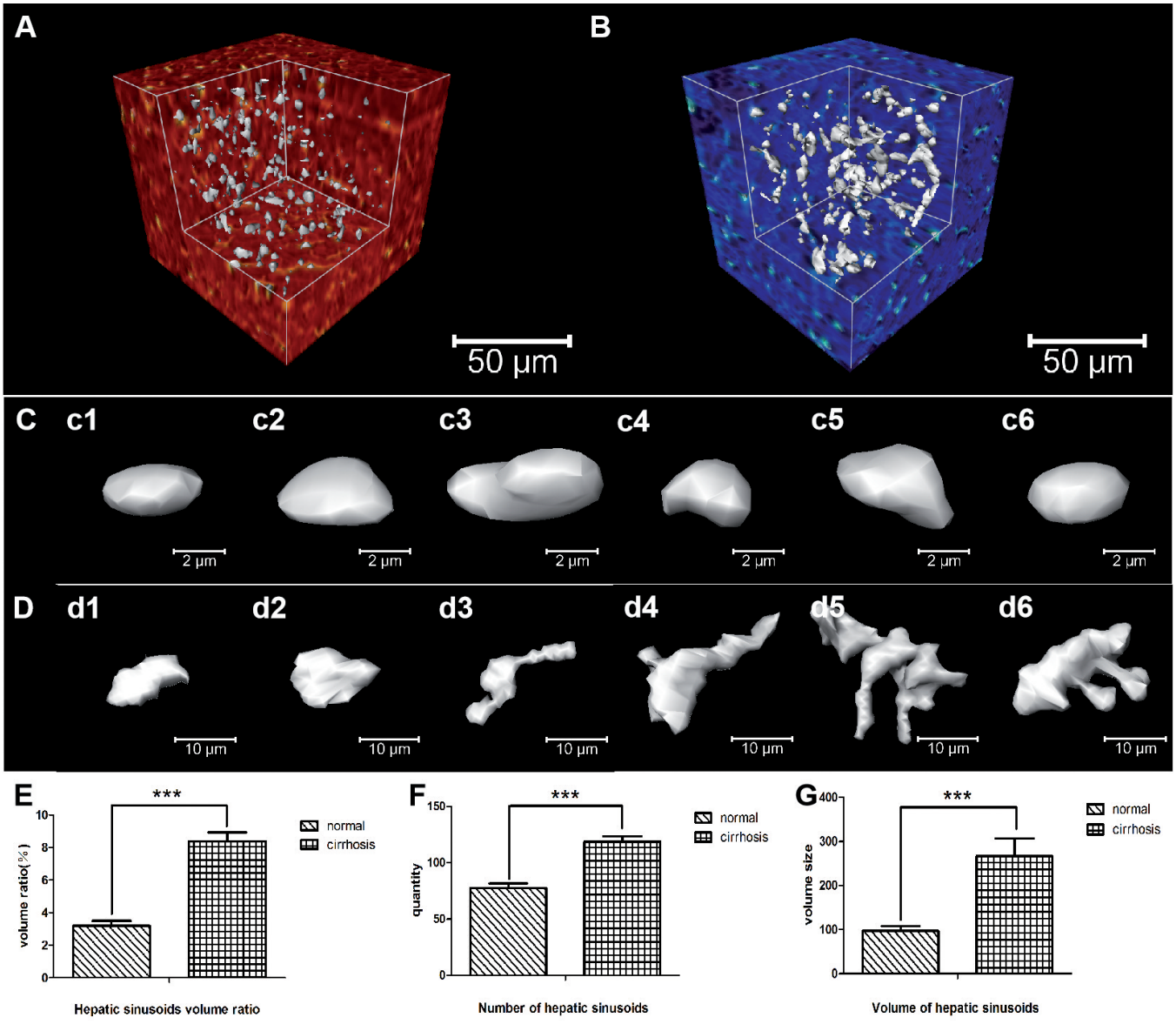

Fig. 4. 3D volume rendering and quantitative analyses of hepatic sinusoids. In the reconstructed VOIs of the normal **(A)** and cirrhotic samples **(B)**, the single sinusoids were segmented and are shown in **C** and **D**, respectively. The quantitative analysis of hepatic sinusoids is summarized in **E-G**. ***P<0.001.

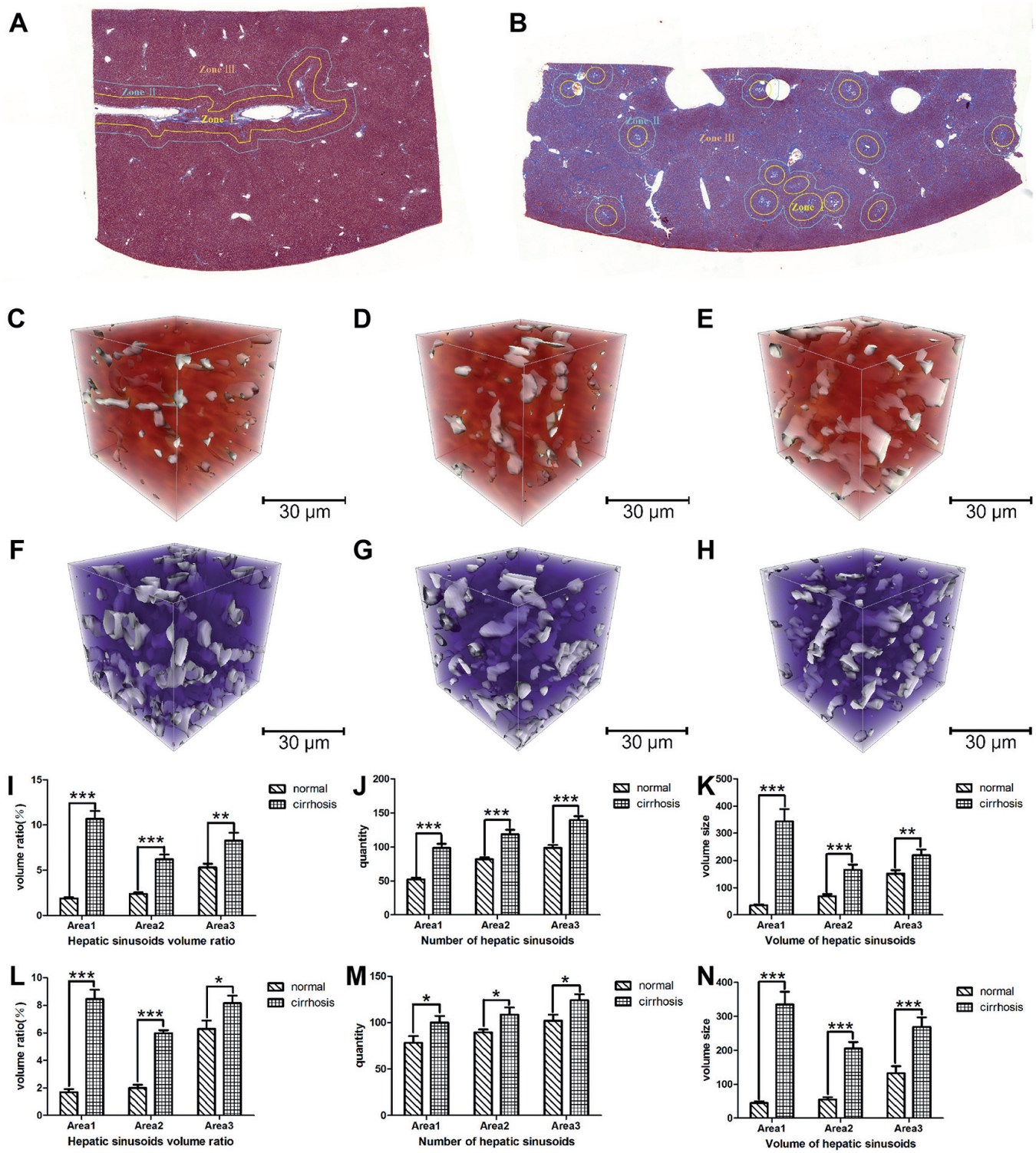

Fig. 5. 3D reconstruction and quantitative analysis of sinusoids in zones I-III. In the sections of normal **(A)** and cirrhotic **(B)** samples, the livers were divided into three zones based on the distance from the portal area. The VOIs of normal and cirrhotic samples of zones I-III are presented in **C-E** and **F-H**, respectively. The morphological parameters of the hepatic sinusoids of the test set and validation set are provided in **I-K** and **L-N**, respectively. *P<0.05;**P<0.01;***P<0.001.

presented in Fig. 5C-E and F-H, respectively. Using the test set, the quantitative parameters of hepatic sinusoids are summarized in Fig. 5I-K. The volume ratios of hepatic sinusoids in zone I, zone II, and zone III of the normal liver sample were 1.89±0.43%, 2.38±0.54%, and 5.30±1.32%, respectively, and that of the cirrhotic sample rose in zones I-III: 10.66±2.81%, 6.20±1.66%, and 8.28±2.71%, respectively ($P<0.05$ between the groups, Fig. 5I), which increased by 4.64- 1.61-, and 0.56-fold, respectively. Similarly, the numbers of hepatic sinusoids of the normal sample in zones I-III were 52.3±6.73, 81.7±9.24, and 98.6±13.91, respectively, and the corresponding values of the cirrhotic sample in the same zones were 98.6±19.16, 118.4±21.06 and 139.4±18.15, respectively. There were 0.89-, 0.45- and 0.41-fold increases in the numbers of sinusoids in the cirrhotic sample compared with the normal liver sample ($P<0.05$ between the groups, Fig. 5J). Additionally, the volumes of single sinusoids of the cirrhotic sample in zones I-III were 343.36±321.95 μm^3, 165.09±138.19 μm^3 and 219.87±147.98 μm^3, and they expanded by 9.9 times, 2.41 times and 1.46 times compared with zone I (34.68±25.91 μm^3), zone II (68.64±53.94 μm^3) and zone III (150.86±95.27 μm^3) in the normal liver sample, respectively ($P<0.05$). Furthermore, the experiment was performed using a validation set, and the same conclusions were confirmed (Fig. 5L-N).

Discussion

In this study, the fine structures of hepatic sinusoids of normal and cirrhotic samples of rats were reconstructed three-dimensionally using serial section reconstruction, and the results provided clear insight into the observation of the collagen distribution and the morphological changes of sinusoids, which contributes to the understanding of the pathology and microstructure of hepatic sinusoids. Compared with CLSM, TEM, SEM and other optical microscopes, 3D reconstruction by serial histological sections can overcome the limitations of the sample size and thickness and present the 3D morphology of the inner microstructure in large samples. In this study, the 3D microstructure of hepatic sinusoids was clearly presented in the normal and cirrhotic samples (approximately $1/10^{th}$ of a liver lobe) instead of liver biopsy (~$1/50{,}000^{th}$ of the total mass of the liver) (Bravo et al., 2001). The adaptive deformations of sinusoids, such as distortion, dilation, proliferation etc., are displayed in detail, and valuable quantitative indicators are provided.

As one of the important metabolic organs, various functions of the liver rely on its basic structure, i.e., liver lobules (Taub, 2004). With the development of fibrosis, fiber content gradually increases, and the proliferating fibrous septations destroy the structure of liver lobules, even leading to the formation of pseudo-lobules. In addition, fibroplasia can also destroy the original structure of hepatic sinusoids and cause cell metabolism and substance exchange disorders (Martinez-hernandez, 1984; Clement et al., 1986; Biagini and Ballardini, 1989). Hepatic sinusoids are interlobular microvessels, and their morphological changes are closely related to liver injury and regeneration (Sasa-Marcel et al., 2005). In this study, 3D reconstructions of the fine structures of fibers and parenchyma have been presented, and fibrosis areas were measured. The hyperplastic fibres caused by cirrhosis destroy the structure of the lobules and cause the formation of pseudolobules. Compared with normal liver, cirrhosis causes expansion and tortuosity of sinusoids and corrugation of the sinusoid surface. Moreover, normal sinusoids present actinomorphic distribution near the central vein, which is beneficial for blood flow back to the central vein. In contrast, the disordered distribution of cirrhotic sinusoids is revealed clearly, and the 3D structures of sinusoids are significantly changed compared with normal sinusoids, which may lead to increased vascular resistance (Shimizu and Yokoyama, 1993).

In addition, the sections were divided into three zones to further investigate the morphological differences of hepatic sinusoids according to the transportation of nutrients. This study demonstrates that cirrhosis leads to different degrees of increase in sinusoidal volume ratio, number of sinusoids, and single sinusoid volume in all zones as a diffuse liver disease. The enlarged sinusoid volume in cirrhosis accelerates blood flow, and the nutrients in blood cannot be fully absorbed by hepatocytes. As the distance from the portal area increases, the number of sinusoids in normal and cirrhotic livers gradually increases. There were significant differences between the groups in the number of hepatic sinusoids at the same zones, indicating that the increased sinusoidal number is one of the main manifestations of cirrhosis. In addition, the sinusoid volume ratio was positively correlated with the number and volume of a single hepatic sinusoid. Especially for cirrhosis, the most significant increase in the sinusoidal volume ratio and the volume of a single sinusoid were presented in zone I, and the sinusoids in zone I were more prone to adaptive variation because of the more abundant blood supply and oxygen content. Obviously, abnormal morphological changes of hepatic sinusoids result in obstacles to material exchange in cirrhotic tissue.

While the preliminary results are encouraging, there are some limitations. First, only one case each of normal and cirrhotic rats was selected. The human serum albumin-induced cirrhosis model is of immune cirrhosis and is similar to clinical cirrhosis in terms of pathogenic factors. Its advantages lie in stable formation and less damage to hepatocytes, which is conducive to in situ observation. However, it is necessary to investigate more cirrhosis models caused by different diseases to explore the adaptive remodelling of liver microstructure in different types of liver injury. Second, immersion fixation was used for preservation of liver tissue in this study, as performed in previous studies (Shimizu et al., 1996; Duan et al., 2013a,b; Yoon et al., 2013). However,

immersion fixation whilst standard in histopathology is not ideal for preservation of liver tissue due to the possibility of sinusoidal collapse, which needs to be improved in future research. Third, the number of consecutively registered sections is less than 200 due to limitation of registration. The accumulation of deformation errors in the registration process may cause image distortions in late stage of registration and decrease registration quality. To obtain clearer 3D visualization and more comprehensive analysis of the large sample structure, more effective registration methods need be explored in future research.

In summary, our research accurately reconstructed and analysed the 3D morphological structure of hepatic sinusoids in cirrhotic rats by serial histological sections. The adaptive changes in sinusoid morphology were clearly displayed, and the proliferation of fibres was visualized in a 3D manner. Accurate 3D visualization of hepatic sinusoids based on histology could be a valuable method for evaluating morphological changes and has important reference value for exploration of microcirculation and pathological features of cirrhosis.

Funding. The National Natural Science Foundation of China (grant Nos. 81671683, 81670545, 82071922, and 81371549); The Natural Science Foundation of Tianjin City in China (grant No. 16JCYBJC28600); Tianjin Research Innovation Project for Postgraduate Students (2019YJSS169).

Conflicts of Interest. The authors have no conflict of interest to declare.

References

Adams C.M., Danks D.M. and Campbell P.E. (1974). Comments upon the classification of infantile polycystic diseases of the liver and kidney, based upon three-dimensional reconstruction of the liver. J. Med. Genet. 11, 234-243.

Araki M., Kawashima S., Matsumoto N., Nishimura S., Ishii T., Komiyama K. and Honda K. (2010). Three-dimensional reconstruction of a fibro-osseous lesion using binary images transformed from histopathological images. Dentomaxillofac. Radiol. 39, 246-251.

Biagini G. and Ballardini G. (1989). Liver fibrosis and extracellular matrix. J. Hepatol. 8, 115-124.

Booth M.E., Treanor D., Roberts N., Magee D.R., Speirs V. and Hanby A.M. (2015). Three-dimensional reconstruction of ductal carcinoma in situ with virtual slides. Histopathology 66, 966-973.

Bravo A.A., Sheth S.G. and Chopra S. (2001). Liver biopsy. N. Engl. J. Med. 344, 495-500.

Brunt E.M., Gouw A.S.H., Hubscher S.G., Tiniakos D.G., Bedossa P., Burt A.D., Callea F., Clouston A.D., Dienes H.P., Goodman Z.D., Roberts E.A., Roskams T., Terracciano L., Torbenson M.S. and Wanless I.R. (2014). Pathology of the liver sinusoids. Histopathology 64, 907-920.

Carazo J.M., Ortiz-de-Solorzano C. and Kybic J. (2006). Consistent and elastic registration of histological sections using vector-spline regularization. In: Computer vision approaches to medical image analysis. CVAMIA 2006. Beichel R.R. and Sonka M. (eds). Springer Berlin Heidelberg, Berlin, Heidelberg. 85-95.

Cheng D., Morsch M., Shami G.J., Chung R.S. and Braet F. (2019). Albumin uptake and distribution in the zebrafish liver as observed via correlative imaging. Exp. Cell Res. 374, 162-171.

Cheng W., Ge Q., Wan L., Wang X., Chen X. and Wu X. (2017). A method to establish a mouse model of bone marrow microenvironment injury. Exp. Anim. 66, 329-336.

Clement B., Grimaud J.L., Campion J.I., Deugnier Y. and Guillouzo A. (1986). Cell types involved in collagen and fibronectin production in normal and fibrotic human liver. Hepatology. 6, 225-234.

Crum W.R., Hartkens T. and Hill D.L.G. (2004). Non-rigid image registration: theory and practice. Br. J. Radiol. 77, S140-S153.

Duan J., Hu C. and Chen H. (2013a). High-resolution micro-CT for morphologic and quantitative assessment of the sinusoid in human cavernous hemangioma of the liver. PLos One 8, e53507.

Duan J., Hu C., Luo S., Zhao X. and Wang T. (2013b). Microcomputed tomography with diffraction-enhanced imaging for morphologic characterization and quantitative evaluation of microvessel of hepatic fibrosis in rats. PLos One 8, e78176.

Hoehme S., Brulport M., Bauer A., Bedawy E., Schormann W., Hermes M., Puppe V., Gebhardt R., Zellmer S., Schwarz M., Bockamp E., Timmel T., Hengstler J.G. and Drasdo D. (2010). Prediction and validation of cell alignment along microvessels as order principle to restore tissue architecture in liver regeneration. P. Natl. Acad. Sci. USA 107, 10371-10376.

Jansen I., Lucas M., Savci-Heijink C.D., Meijer S.L., Liem E.I.M.L., de Boer O.J., van Leeuwen T.G., Marquering H.A. and de Bruin D.M. (2019). Three-dimensional histopathological reconstruction of bladder tumours. Diagn. Pathol. 14, 25.

Kleiner D. (2009). The pathology of drug-induced liver injury. Semin. Liver Dis. 29, 364-372.

Martinez-hernandez A. (1984). The hepatic extracellular matrix. I. Electron immunohistochemical studies in normal rat liver. Lab. Invest. 51, 57-74.

Meyer K., Ostrenko O., Bourantas G., Morales-Navarrete H., Porat-Shliom N., Segovia-Miranda F., Nonaka H., Ghaemi A., Verbavatz J., Brusch L., Sbalzarini I., Kalaidzidis Y., Weigert R. and Zerial M. (2017). A predictive 3D multi-scale model of biliary fluid dynamics in the liver lobule. Cell Syst. 4, 277-290.

Micheva K.D., O'Rourke N., Busse B. and Smith S.J. (2010). Array tomography: High-resolution three-dimensional immuno-fluorescence. Cold Spring Harbor Protocols 2010, p89.

Nie Q., Zhu C., Zhang Y., Yang J., Zhang J. and Gao R. (2010). Inhibitory effect of antisense oligonucleotide targeting TIMP-2 on immune-induced liver fibrosis. Digest. Dis. Sci. 55, 1286-1295.

Nonomura A., Ohta G., Yoshida K., Kurachi M., Matsubara F. and Takazakura E. (1978). Congenital hepatic fibrosis. A case report with study of three dimensional reconstruction of serial sections of the liver. Acta Pathol. Jpn. 28, 949-956.

Onori P., Morini S., Franchitto A., Sferra R., Alvaro D. and Gaudio E. (2000). Hepatic microvascular features in experimental cirrhosis: a structural and morphometrical study in CCl_4-treated rats. J. Hepatol. 33, 555-563.

Peeters G., Debbaut C., Laleman W., Monbaliu D., Vander Elst I., Detrez J.R., Vandecasteele T., De Schryver T., Van Hoorebeke L., Favere K., Verbeke J., Segers P., Cornillie P. and De Vos W.H. (2017). A multilevel framework to reconstruct anatomical 3D models of the hepatic vasculature in rat livers. J. Anat. 230, 471-483.

Rappaport A.M., Black R.G., Lucas C.C., Ridout J.H. and Best C.H. (1966). Normal and pathologic microcirculation of the living

mammalian liver. Rev. Int. Hepatol. 16, 813-828.

Saatchi S., Wanchoo N., Azuma J., Smith S.J., Tsao P.S., Yock P.G. and Taylor C.A. (2011). The use of immunofluorescent array tomography to study the three-dimensional microstructure of murine blood vessels. Cell Mol. Bioeng. 4, 311-323.

Sasa-Marcel M., Eduard R., Zilfi U.L., Martha M.G. and Jan S. (2005). Disturbance of hepatic and intestinal microcirculation in experimental liver cirrhosis. World J. Gastroenterol. 11, 846-849.

Schneider C.A., Rasband W.S. and Eliceiri K.W. (2012). NIH image to ImageJ: 25 years of image analysis. Nature Meth. 9, 671-675.

Shimizu H. and Yokoyama T. (1993). Three-dimensional structural changes of hepatic sinusoids in cirrhosis providing an increase in vascular resistance of portal hypertension. Acta Pathol. Jpn. 43, 625-634.

Shimizu H., Suda K. and Yokoyama T. (1996). Difference in the three-dimensional structure of the sinusoids between hepatocellular carcinoma and cirrhotic liver. Pathol. Int. 46, 992-996.

Tanaka M., Tanaka K., Masaki Y., Miyazaki M., Kato M., Kotoh K., Enjoji M., Nakamuta M. and Takayanagi R. (2014). Intrahepatic microcirculatory disorder, parenchymal hypoxia and NOX4 upregulation result in zonal differences in hepatocyte apoptosis following lipopolysaccharide- and D-galactosamine-induced acute liver failure in rats. Int. J. Mol. Med. 33, 254-262.

Taub R. (2004). Liver regeneration: from myth to mechanism. Nat. Rev. Mol. Cell Bio. 5, 836-847.

Teutsch H.F., Schuerfeld D. and Groezinger E. (1999). Three-dimensional reconstruction of parenchymal units in the liver of the rat. Hepatology 29, 494-505.

Titze B. and Genoud C. (2016). Volume scanning electron microscopy for imaging biological ultrastructure. Biol. Cell 108, 307-323.

Tolkach Y., Thomann S. and Kristiansen G. (2018). Three-dimensional reconstruction of prostate cancer architecture with serial immunohistochemical sections: hallmarks of tumour growth, tumour compartmentalisation, and implications for grading and heterogeneity. Histopathology 72, 1051-1059.

Vollmar B. and Menger M.D. (2009). The hepatic microcirculation: Mechanistic contributions and therapeutic targets in liver injury and repair. Physiol. Rev. 89, 1269-1339.

Wang B. (1989). Animals with liver fibrosis induced by albumin immunization. Zhonghua Yi Xue Za Zhi. 69, 503-505, 36.

Wang F.S., Fan J.G., Zhang Z., Gao B. and Wang H.Y. (2014). The global burden of liver disease: The major impact of China. Hepatology 60, 2099-2108.

Wang Y., Chen S., Ni Y., Magee D., Pu Y., Zhou Q., Wang Z., Zhang L., Huang X. and Hu Q. (2018). Three-dimensional reconstruction with serial whole-mount sections of oral tongue squamous cell carcinoma: A preliminary study. J. Oral Pathol. Med. 47, 53-59.

Yoon Y.J., Chang S., Kim O.Y., Kang B.K., Park J., Lim J.H., Yun H.J., Kim Y.K., Byun J.H. and Gho Y.S. (2013). Three-dimensional imaging of hepatic sinusoids in mice using synchrotron radiation micro-computed tomography. PLos One 8, e68600.

Zhang R., Huang X.Q., Jiang Y.Y., Li N., Wang J. and Chen S.Y. (2020). LncRNA TUG1 regulates autophagy-mediated endothelial-mesenchymal transition of liver sinusoidal endothelial cells by sponging miR-142-3p. Am J. Transl. Res. 12, 758-772.

Zhao X., Wang B., Li X. and Wang T. (2008). Newly proposed fibrosis staging criterion for assessing carbon tetrachloride- and albumin complex-induced liver fibrosis in rodents. Pathol. Int. 58, 580-588.

Accepted April 14, 2021